Vol.7 No.1 Jan 2024

Multimedia Research

Received 10 November, Revised 18 November, Accepted 15 December

Deep Learning based Time Series Classification Model for Monitoring Land Cover Changes in Tropical High Forests

K. Chandra Shekar

Associate Professor, Department of CSE
Guru Nanak Institutions Technical Campus (Autonomous)
Ibrahimpatnam, Hyderabad, Telangana, India
chandhra2k7@gmail.com

Abstract: The monitoring of land cover/use in city areas is more important to have timely, accurate, and effective utilization and development of urban land resources. This remotely sensed dynamic monitoring greatly depends on the remote sensing data at high spatial and temporal resolutions. Still, the influence of weather and revisiting periods make time series images more complex. In this paper, a new land cover change detection model is implemented with three major three processes: Pre-processing, Detection of forest region, and Change detection of the forest. Initially, the input image is subjected to median filtering for outlier removal, reducing the influence of low-quality data and also filtering the noise. Once the image gets pre-processed, it is subjected to the detection of forest in the image by the optimized Convolutional Encoder-Decoder (OCED). The OCED classifier separates the forest region from the image as it resides with the cover of land, water, and forest as well. To make the process more effective, OCED gets enhanced by tuning the weight, and activation function are fine-tuned by the new algorithm termed as, Averaged Distance-based Sea Lion Optimization (ADSLnO) algorithm. Subsequently, the detected forest region is subjected to DTW-based time-series classification, which makes the year-wise change detection of the years 2007, 2009, 2015, and 2017. Finally, the performance of the adopted model is analyzed over other existing approaches in terms of certain metrics such as NPV, sensitivity, FDR, accuracy, specificity, FPR, precision, MCC, FNR, and F1-score, respectively.

Keywords: Land Cover Change Detection; Pre-Processing; Forest Region Detection; Forest Change Detection; Optimization.

Nomenclature

Abbreviation	Description
AGDD	Accumulated Growing Degree-Days
ADSLnO	Averaged Distance-based Sea Lion Optimization
CUSUM	Cumulative Sum
CNN	Convolutional Neural Network
DD	Detection Delay
DTW	Dynamic Time Warping
DBN	Deep Belief Network
ESTARFM	Enhanced Spatial and Temporal Adaptive Reflectance Fusion Model
EVI	Enhanced Vegetation Index
ETM	Enhanced Thematic Mapper
FDR	False Discovery Rate
FNR	False Negative Rate
FPR	False Positive Rate
GEOBIA	Geographic Object-Based Image Analysis
GWO	Grey Wolf Optimization
LULC	Land-Use/Land-Cover
MCC	Matthews Correlation Coefficient
OCED	Optimized Convolutional Encoder-Decoder
OLI_TIRS	Operational Land Imager/Thermal Infrared Sensor
PCA	Principal Component Analysis
PF	Particle Filter
RF	Random Forest
SITS	Satellite Image Time Series
SLnO	Sea Lion Optimization
ST-MRS	Spatiotemporal Multi-Resolution Segmentation
SPOT	Satellite Pour l'Observation de la Terre

https://doi.org/10.46253/j.mr.v7i1.a3

TM	Thematic Mapper
TSCCD	Time-Series Classification approach based on Change Detection
2D	Two-Dimensional
WOA	Whale Optimization Algorithm
EBTSA	Ensemble of Bidirectional Time Series Analysis
CCDC	Continuous Change Detection and Classification
LST	Land Surface Temperature
DEM	Digital Elevation Model
SAVI	Soil Adjusted Vegetation Index
NDVI	Normalized Difference Vegetation Index
ReLU	rectified linear non-linearity

1. Introduction

The land use/cover information plays an important role in the planning, management, reasonable development of land, and dynamic monitoring [9] [10]. In recent times, the land cover information that occurred from satellites gets altered in and out of the cities. This is due to the quicker urban expansion, and most of the time, the construction land is increasingly scarce, and non-agriculturalization of arable land is highlighted [11] [12]. The SITS indicated a group of image data from satellite sensors for a similar geographical area across time [13] [14] [15]. The SPOT, IKONOS, Sentinel-2, and Landsat-8 have increased the availability of high-resolution images (both temporally and spatially) with the advancement of remote sensing sensors. Further, this drives the requirement for information like temporal and phenological evolutions, spatial changes from SITS, and land-cover semantics. Along with this, the urban thermal environment, ecosystem carbon cycle, hydrology, and analyzing and monitoring of land uses/covers changes are mostly used in the SITS[16] [17] [18].

Nowadays, Earth observation satellites can collect data within short revisit periods and can be extensively used to detect and monitor the changes in land cover. In land cover time series, Fourier analysis is used for extracting the constraints providing the features of the land cover class types [19] [20]. Still, these constraints do not capture the variations in land cover with time, particularly, the inter-annual similarities related to the seasonality. Time–series models are the most commonly used techniques for the Earth observation variables, particularly for understanding the inter-interannual variations [21] [22]. Furthermore, the techniques [37] [35] are used for vegetation-related research as they have extensive temporal and spatial coverage.

To improve the performance of change detection with SITS, the spatiotemporal heterogeneity selects suitable spatiotemporal scales and correlations. GEOBIA is implemented to eliminate the spectral heterogeneity of geographic objects with superior outcomes and attains the per-pixel model via the analysis of single-date images [23] [24]. Nevertheless, the GEOBIA adaptation to SITS is becoming more complex to exploit both the temporal and spatial information. In SITS, the new types of units are required other than the pixels to represent the geographic objects. Nowadays, deep learning [31] [32] [33] [36] [34] techniques are most commonly used for the detection of land cover changes. The major contribution of the adopted work is listed below:

- Proposed an Averaged Distance-based Sea Lion Optimization (ADSLnO) algorithm for training the OCED model via selecting the optimal weights and activation function.

In this paper, Section 2 indicates the literature review on land cover change detection. Section 3 signifies the monitoring land cover changes in tropical high forests: a deep learning-based time series classification model. Section 4 portrays the pre-processing and optimized deep learning-based forest segmentation or separation. Section 5 delineates the DTW for time series classification. The results and their discussions are determined in Section 6. At last, section 7 concludes the paper.

2. Literature Review

2.1 Related Works

In 2019, Yan *et al.* [1] presented an effectual approach based on TSCCD for speedy LULC mapping. Here, the model was deployed for recognizing the time-series segmentation, and changes in land cover were detected. In addition, the DTW approach was exploited for classifying the sub-time series. The experimentations have revealed that the presented method significantly enhanced the feasibility and efficiency over the conventional schemes.

In 2019, Lossou *et al.* [2] designed a mechanism that deployed the “multi-temporal optical remote sensing and spatial analytical” frameworks for assessing the position of 8 forest reserves in the “tropical

high forests of Ghana under the management of the Goaso Forest District. Landsat data of 1990 TM, 2013 ETM+, and 2017 OLI_TIRS were classified into closed-canopy forest, open-canopy forest, bare land/built-up, farmland, and degraded land using the Maximum Likelihood algorithm". Furthermore, the outcomes demonstrated that the designed model has ensured an effective method for curbing the forest depletion rates in Ghana.

In 2019, Xi *et al.* [3] presented a spatiotemporal cube framework with an ST-MRS technique for examining the SITS. Initially, the new spatiotemporal scheme called ST-cube was modeled for reducing the spectral heterogeneities in temporal and spatial domains. Subsequently, the ST-MRS technique aids in segmenting the SITS into comparatively standardized ST cubes. Further, an unsupervised technique (ST-MRS) was used for evaluating the results of segmentation.

In 2019, Deng *et al.* [4] suggested an ESTARFM for blending the "Landsat8 and MODIS data" and it obtained the "time-series Landsat8 images". Subsequently, land cover data was extracted using an object-oriented classification technique. Here, the presented model was confirmed using a case study in Changsha City. Further, the performance of the adopted technique has attained better outcomes concerning accuracy and efficiency.

In 2018, Chakraborty *et al.* [5] presented a method for detecting the rapid variations in land cover and capturing the time-varying occurrences of vegetation in the growth cycle due to forest fires. In addition, a "sequential Monte Carlo estimation approach of the time-varying frequency" was designed using the PF. A binary hypothesis land cover detector was implemented, which depends on a divergence measure among varied time series noticed throughout the months of successive years. The simulated outcomes have demonstrated the enhancement of the presented technique with minimal delay.

In 2019, Olding *et al.* [6] introduced a design for online recognition of land cover variations depending on time series. Variations were noticed by observing the changes among forecasts and observations made using the time series of geographical regions and historical data. This technique and numerous other techniques were deployed to "MODIS 8-day surface reflectance data for the problems of detecting settlement expansion in Limpopo Province, South Africa, and detecting deforestation in New South Wales, Australia". The attained outcomes have illustrated the superiority of the established scheme in terms of reduced DD.

In 2020, Lan *et al.* [7] developed a technique for mapping land cover by exploiting "multi-temporal Earth Observation data from Landsat and MODIS". Here, a yearly time series was built by AGDD from a composite of temperatures observed from the land surface. In addition, by deploying the EVI, a convex quadratic framework was fitted at every pixel for to year-wise evolution of AGDD. Finally, simulations were done and the established model has revealed better accuracy when compared to the existing model.

In 2019, Márquez *et al.* [8] presented a unique predictor variable for predicting the spatio-temporal LULC variations. Here, the adopted tools have portrayed the changes among predicted and observed variables by examining the prediction concerning various error measures. The predicted outcomes of LULC variations via the PC1 forecast were used for determining diverse future time series. Furthermore, the analysis of prediction has demonstrated the superiority of the introduced model and it has acquired minimal error measures over other compared models.

In 2022, Rehan Khan *et al.* [42] studied variations in surface temperature (land) that affect LULC. They used the Maximum Likelihood Classification technique to classify LULC in Landsat satellite pictures. The NDVI was then used to calculate LST based on LULC changes to determine the degree of vegetation degradation. The results also showed a growth in arid regions, a drop in forest areas, and a rise in built-up areas. This led to a rise in LST and natural resources.

In 2022, Baohui Chai *et al.* [43] introduced the EBTSA technique to inspect the variations in the land cover of the urban surroundings through Landsat data. Initially, it combined two techniques: the Chow Test and CCDC. The three steps of the process were break detection with CCDs, alteration in the Chow test, and classification or incorporation with a bidirectional model to monitor and detect the changes. This improved accuracy and reduced errors while detecting. The overall results showed improvements in spatial and temporal accuracy in both classifications as well as change detection. Finally, the analysis revealed that there had been rapid expansion along with a transition from vegetation towards urban lands accompanied by diverse changes between various nonurban cover types, thus showcasing the effectiveness of the EBTSA approach for better understanding the dynamics behind such landcover changes.

In 2022, Yunwei Tang *et al.* [44] monitored changes in land cover and historic sites using semi-automatic two-level processes and very high-resolution bi-temporal remote sensing technology. The protection condition of these CHS was analyzed using an indicator called interference degree and then monitored over time. Depending on the High-resolution Google Maps images, three types of CHS, such as ancient temples, antiquity building features, and ancient sites, were examined. Finally, the outcome offered the possibility of producing global CHS data that could aid in achieving the target outlined in the Goals for Sustainable Development.

In 2022, Saeid Amini *et al.* [45] focused on classifying land cover and use using remote sensing images. For classification tasks, they primarily used the Random Forest classifier. Landsat imagery served as input for Google Earth throughout implementation. To reduce the multispectral pixel density of Landsat bands from 30m to 15m, pan-sharpening algorithms were investigated. The effects of image compositions differ based on spectral indices, including the DEM and LST. On the final accuracy, LULC mapping results were also investigated. Overall, the results were more accurate, and they can be quickly and simply applied to other areas.

In 2022, Md. Sazzad Hossain *et al.* [46] have estimated almost three decades, for changes in LULC in Bangladesh (FKWS). They employed a maximum likelihood algorithm to detect change using several remotely sensed data from Landsat satellite images. The comparative potential of very clear indicators of the level of water stress in the crops like the Landsat SAVI and remote sensing measurements like NDVI for assessing forest cover were also examined. A significant loss was recorded through deforestation due to agricultural activities like land conversion into bare land by rural communities depending on household agriculture for livelihoods. NDVI provided better accuracy than SAVI when it came to assessing forest covers, which can be useful while monitoring future impacts caused by various types of land use changes. Finally, the increase and decrease of two variables (NDVI and LST) were found and verified for the contribution of global warming to forest damage.

2.2 Review

Table 1. *Review on conventional land cover change detection model in time series: Features and Challenges*

Author [citation]	Adopted scheme	Features	Challenges
Yan *et al.* [1]	DTW model	✓ Handles missing data and noise ✓ Robust approach	➢ It is not appropriate for satellite images with higher resolution.
Lossou *et al.* [2]	Maximum Likelihood algorithm	✓ Better accuracy ✓ Minimal error	➢ Have to consider more on cost factors.
Xi *et al.* [3]	ST-MRS model	✓ Highly accurate ✓ Reduced random noise	➢ Should focus on time efficiency.
Deng *et al.* [4]	ESTARFM method	✓ High accuracy ✓ Better efficiency	➢ Uncertainties occur from ➢ the fused images
Chakraborty *et al.* [5]	PF Model	✓ Minimal error ✓ Improved spatial scalability	➢ Can be extended to other types of change events.
Olding *et al.* [6]	CUSUM algorithm	✓ Reduced delay ✓ Faster approach	➢ Need to reduce the occurrence of false alarms, and the DD.
Lan *et al.*[7]	RF classifier	✓ Increased quality ✓ High accuracy	➢ Output stability has to be considered more.
Márquez *et al.*[8]	PCA	✓ Minimal error ✓ Optimal prediction	➢ Disturbances occur due to the interference of clouds in the scene.
Rehan Khan *et al.* [42]	Maximum likelihood classification	✓ It is a cost-effective, efficient way to assess LST changes over time. ✓ Identified areas that require attention from policymakers or conservationists.	➢ Only covers two districts. ➢ Does not provide insights.
Baohui Chai *et al.* [43]	EBTSA	✓ Improved the robustness against data scarcity in earlier times while reducing break detection errors. ✓ Capable of both change detection and classification with improved spatial-temporal accuracies.	➢ Evaluated only one area. ➢ Did not consider additional factors such as climate or socio-economic changes.
Yunwei Tang *et al.* [44]	OBIA	✓ Allows efficient extraction. ✓ Results are less subjective and more objective than manual interpretation.	➢ Limited sample size ➢ Reliance on Google Earth images ➢ Lack of ground-truthing validation. ➢ No comparison with existing methods.
SaeidAmini*et al.* [45]	RF, GEE, and Pan-sharpening algorithm	✓ The use of pan-sharpened top-of-atmosphere Landsat products increased accuracy.	➢ Tested only on Landsat data ➢ The study area was limited to a specific region.
Md. Sazzad Hossain *et al.* [46]	NDVI, SAVI, LST and Landsat imagery.	✓ Accurate land cover classification. ✓ Effective change detection ✓ Better assessment with NDVI index. ✓ Understand the climate impact of forests.	➢ Lack of ground truth data ➢ Limited scope ➢ No analysis for underlying causes

Table 1 demonstrates the review on land cover change detection in time series. Initially, the DTW model was presented in [1] that offers a robust approach and it handles missing data and noise in a better manner. Nevertheless, it is not appropriate for satellite images with higher resolution. The maximum Likelihood algorithm was developed in [2] that reduces error with better storage accuracy, but it has to consider more cost factors. In addition, the ST-MRS model was used in [3], which provides minimal noise and is highly accurate; nevertheless, it should focus on time efficiency. Also, the ESTARFM method was employed in [4] that provides high accuracy with better efficiency. However, uncertainties occur from the fused images. Likewise, the PF model was presented in [5] that offers enhanced spatial scalability with minimal error. However, it can be extended to other types of change events. In addition, Page's CUSUM algorithm was deployed in [6] that ensure reduced delay and it is a faster approach. Nevertheless, need to reduce the occurrence of false alarms and the DD. RF classifier was deployed in [7] that provides increased quality and high accuracy, however, output stability has to be considered more. PCA was presented in [8] that offers reduced error with optimal prediction; but, disturbances occur due to the interference of cloud in the scene. There, these limitations have to be considered for improving the land cover change detection in time series effectively in the current research work.

3. Monitoring Land Cover Changes in Tropical High Forests: A Deep Learning-based Time Series Classification Model

This paper introduces deep learning-based land cover change detection in tropical high forests. The proposed architecture is illustrated in Fig 1, which includes three phases: Pre-processing, Detection of forest region, and Change detection of the forest. The first step is pre-processing, where the input image is subjected to median filtering for outlier removal, reducing the influence of low-quality data and also aiding in filtering the noise as well. Once the image gets preprocessed, it is subjected to the detection of the forest. This forest detection process is carried out by the OCED. The classifier separates the forest region from the image as it resides with the cover of land, water, and forest as well. The deep learning classifier can separate/segment the forest regions. To make the forest separation more precise, OCED gets enhanced with the metaheuristic ADSLnO algorithm via tuning the training parameters and activation function. Subsequently, the detected forest region is subjected to DTW-based time-series classification, which makes the year-wise change detection come under the years 2007, 2009, 2015, and 2017. Fig. 1 illustrates the overall architecture of the proposed work.

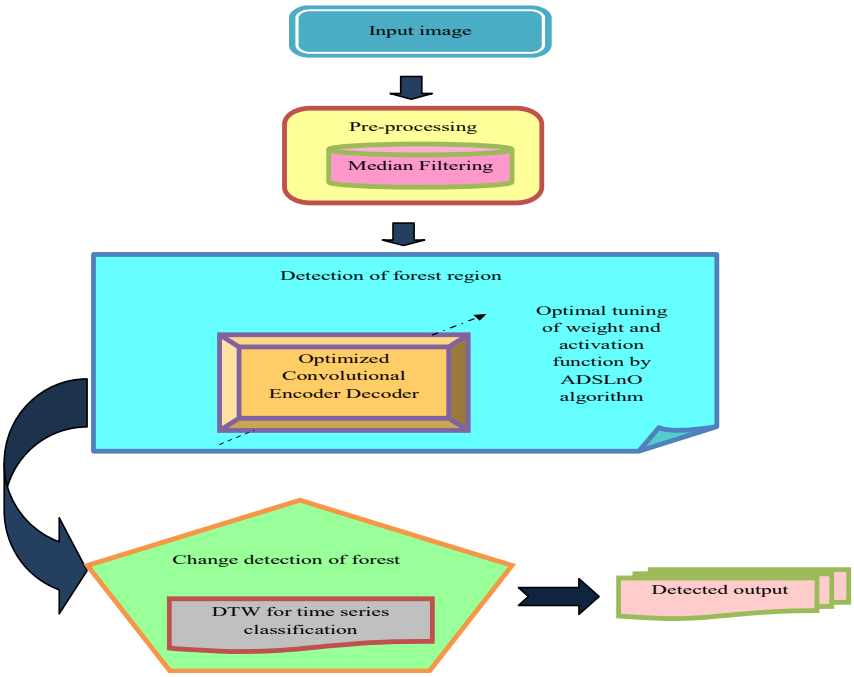

Fig.1.*The overall architecture of the proposed work*

4. Preprocessing and Optimized Deep Learning-based Forest Segmentation or Separation

4.1 Preprocessing

In the preprocessing phase, the median filter is used. Moreover, the noisy value or the digital image sequence is replaced through the (neighborhood) mask of the median value. Based on the gray levels, the pixels of the neighbor are ranked and stored in the grouped median value that replaces the noisy value. Further, $f(u,v)=med\{g(u-l,v-m)l,m\in E\}$ is the output of the median filtering, where, $f(u,v)$, and $g(u,v)$ refers to the output image and the original image, correspondingly, E indicates the 2D mask, $M\times M$ denotes the mask size (i.e.), M is normally odd includes 3×3, 5×5, etc. Further, the shape of the mask is cross, circular, square, and linear, etc.

Lowering the noise performance: The median filter is relatively difficult for the image with random noise, and it is also considered a nonlinear filter. In the median filtering, the noise variance under normal distribution with zero mean noise of an image is given in Eq. (1).

$$\sigma_{med}^2=\frac{1}{4MF^2(M)}\approx\frac{\sigma_l^2}{M+\frac{\pi}{2}-1}.\frac{\pi}{2} \tag{1}$$

In Eq. (1), M refers to the size of the median filtering mask, σ_l^2 indicates the variance of input noise power, $F(M)$and denotes the noise density function. In the average filtering, the noise variance is expressed in Eq. (2).

$$\sigma_o^2=\frac{1}{M}\sigma_l^2 \tag{2}$$

The effects of median filtering depend on the noise distribution and the mask size while comparing Eq. (1) and Eq. (2). Further, the performance of the median filtering provides low random noise, and it is superior to the performance of the average filtering. Still, the pulse width is less than $M/2$, the more effective median filter, and apart narrow pulses have occurred in the impulse noise. When the average filtering algorithm combines with the median filtering algorithm, the performance of the average filtering is increased, and can resize the mask based on the density of noise.

4.2 Optimized Convolutional Encoder-Decoder for Forest Separation

The encoder network includes 13 convolutional layers in OCEN. In the VGG16 network, the 1st 13 convolutional layers are implemented for the classification of objects. Moreover, the convolution layer includes several convolution kernels for computing the different optimal weights using the feature maps. The complete feature map was determined using numerous kernels. Further, the feature values in the location (x,y) with p^{th} layers matching to n^{th} feature map is represented as $R_{x,y,n}^p$, and it is given in Eq. (3), where, the optimal weight vector and the bias term are indicated as w_n^p and b_n^p respectively, and the connected input patches in the n^{th} layer at the location (x,y) is specified as $h_{x,y}^p$.

$$R_{x,y,n}^p=w_n^{pT}h_{x,y}^p+b_n^p \tag{3}$$

The activation value $\left(a_{x,y,n}^p\right)$ is represented in Eq. (4)

$$a_{x,y,n}^p=a\left(R_{x,y,n}^p\right) \tag{4}$$

In addition, the shift-variance in the pooling layer is determined through low resolution in feature maps as in Eq. (5), where, $pool(\ )$ indicates the pooling function, the local neighborhood at the near location (x,y) for every feature map $\left(a_{x,y,n}^p\right)$ is depicted as $S_{x,y}$.

$$Y_{x,y,n}^p=pool\left(a_{x,y,n}^p\right),\forall(C,B)\in S_{x,y} \tag{5}$$

In this work, the weight is optimally tuned by a proposed ADSLnO algorithm. The fully connected layers are discarded by retaining the lower resolution at the deep encoder output of the feature maps. In the OCED encoder network, it lowers the count of parameters from 134M to 14.7M significantly than other frameworks. 13 layers are present in the decoder network, and hence every encoder layer has a nearby decoder layer. Here, the overall decoder outputs are subjected to the soft-max classifier with multi-classes for obtaining the class probabilities in each pixel.

In the encoder network, each encoder performed the convolution process with a filter bank to obtain the feature map sets and it is batch normalized. Moreover, the ReLU $\max(I,J)$ is applied in an element-

wise manner. The max-pooling with stride 2 (i.e.), non-overlapping window, and a 2×2 window is executed and then the resultant outcomes are sub-sampled through factor 2. For achieving the translation invariance, the max-pooling is utilized in the input image over the small spatial shifts. The outcomes of the sub-sampling process in the spatial window provide a huge input image context in the feature map for each pixel. Certain layers of sub-sampling and max-pooling obtain much translation invariance for robust classification with spatial resolution loss in the feature maps. The lossy image representation was increased and it is not used for the segmentation, in which there is a vital boundary delineation. Once the sub-sampling is performed, the store boundary and the captured information are required in the encoder feature maps. After sub sampling, all the encoder feature maps are stored only when the memory is not constrained by inferences. Thus, it is not useful in practical applications, and it is not implemented in an effective way for storing the information. Only the max-pooling indices are stored and in each pooling window, the position of the highest feature value is memorized for every encoder feature map. Moreover, it is performed for each 2×2 pooling window by 2 bits and then stored in an efficient way than the float precision in memorized feature maps. The less memory storage provides outcomes with slight accuracy loss, and it is useful in different applications.

In the decoder network, the suitable decoder up samples from the nearby encoder feature maps by the max-pooling memorized indices in the input feature map, and the spare feature maps are produced during this process. It convolved the trainable decoder filter bank with feature maps for producing dense feature maps. For each map, the batch normalization step is applied. The decoder related to the 1st encoder (i.e.), the nearer input image creates a multi-channel feature map; still, the 3 RGB channels are the encoder inputs. The feature maps are produced in the network with a similar size and number of channels as the encoder inputs, unlike the other decoders. In the final decoder, the output with the large dimensional feature is subjected to a trainable soft-max classifier. Each pixel is classified by this classifier individually. The K channel image with probabilities represents the output of the soft-max classifier. Here, K indicates the classes. At each pixel, the predicted segmentation is related to the class with the highest probabilities. Fig. 2 represents the architecture of the convolutional encoder-decoder network.

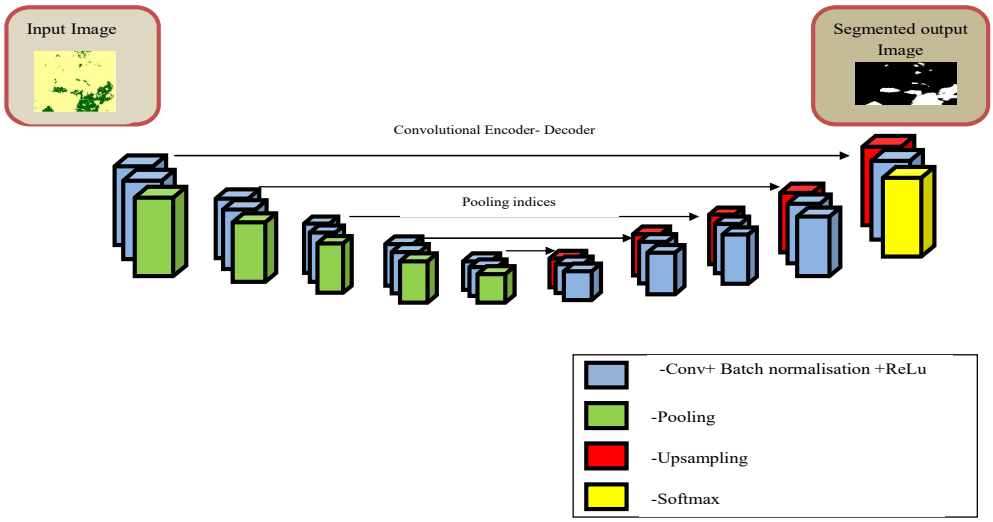

Fig.2. *The architecture of the Convolutional Encoder-Decoder network*

4.3 Objective Function and Solution Encoding

As mentioned, the weights and activation function of OCED is optimized for better detection of forest in the image, where, N refers to the total number of weights in OCED. For the optimal selection of weight, this paper introduces a new hybrid algorithm termed as ADSLnO model. Fig. 3 illustrates the solution encoding process, and the objective function of the implemented method is defined in Eq. (6).

$$Obj = \min\left(error\right) \tag{6}$$

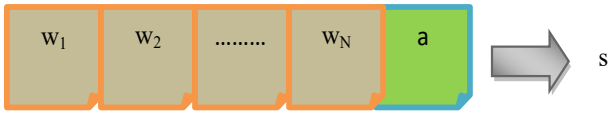

Fig.3. *Solution Encoding*

4.4 Proposed ADSLnO algorithm

Although the traditional SLnO [25] provides a better convergence rate and higher exploitation capability, it is difficult to identify the local optimum points in the search spaces. To tackle this disadvantage of existing SLnO, the algorithm is improved and it is named as ADSLnO algorithm.Generally, self-improvement has proved to be promising for solving many of the complex optimization problems [26] [27] [28] [29] [30]. Sea lions are the best-knowleged species and they can live in huge colonies with more members in the world [26]. The sea lions' functionality is based on their age, sex, and performance of the entire colony. The SLnO algorithm consists of the following phases "detecting and tracking phase, vocalization phase, attacking phase (Exploitation phase) and searching for prey (Exploration phase)".

4.4.1 Identifying and Tracking phase

Sea lions describe the position, shape, and size of the prey using whiskers. Moreover, the whiskers and the path of the water waves are reciprocal to each other, which enables the sea lions to feel the prey and also sense their position. Traditionally in SLnO, the distance is updated among the positions of sea lions and the target prey. The sea lion's behavior is given in Eq. (7).

$$\vec{D}_1 = \left| 2\vec{H}.Q(\vec{t}) - s(\vec{t}) \right| \tag{7}$$

Eq. (7), $\vec{D}$ corresponds to the distance between the sea lions as well as the target prey, and $Q(\vec{t})$ signifies the position vectors of the sea lions and the target prey respectively; t indicates the current iteration and $\vec{H}$ is the random number ranges from [0, 1].Sea lions migrated to nearby target prey in the next iteration, and it is expressed in Eq. (8).

$$s(t+1) = Q(\vec{t}) - \vec{D}.\vec{c} \tag{8}$$

Eq. (8), $(t+1)$ refers to the next iteration and $\vec{c}$ is linearly decreased from 2 to 0 for subsequent iterations.

4.4.2 Vocalization phase

Sea lions are defined to be invertebrates. Sea lions are present on the shore and the water in some cases. The sounds of sea lions travel 4 times faster in the water than in the air. Moreover, they have tiny ears that are effective in sensing noises beneath and above water. Consequently, when a sea lion detects a target, some other sea lions (leaders) are called upon to surround and destroy the prey. The behavior of the sea lion is described in Eq. (9), (10), and (11).

$$S\vec{P}_{leader} = \left| \left(\vec{V}_1 \left(1 + \vec{V}_2 \right) \right) / \vec{V}_2 \right| \tag{9}$$

$$\vec{V}_1 = \sin\alpha \tag{10}$$

$$\vec{V}_2 = \sin\beta \tag{11}$$

Eq. (9), $S\vec{P}_{leader}$ indicates the leader sea lion, $\vec{V}_2$ and $\vec{V}_1$ specifies the speed of sounds in air and water, correspondingly.

4.4.3 Attacking phase (Exploitation phase)

It includes two phases.

a) **Dwindling encircling method**: From Eq. (8), the $\vec{c}$ value depends on the behavior of sea lions, and accordingly the $\vec{c}$ value is reduced randomly from 2 to 0 for further iterations. The arriving position of the search agent is placed somewhere in the desirable position of the current best agent as well as the location of the agent.

b) **Updating Circle position:** Sea lions consume their food by hunting the fish from the edges and chasing them, which is defined in Eq. (12).

$$s(t+1) = \left| \vec{Q}(t) - s(t) \right| .\cos(2\Pi r) + \vec{Q}(t) \tag{12}$$

Eq. (12), $\left| \vec{Q}(t) - s(t) \right|$ indicates the distance between their target prey and the sea lion, | | signifies the correct value and r is the random value ranges among [-1, 1].

4.4.4 Exploration phase

In this phase, sea lions are changing their locations based on the best searching agent. Nevertheless, during the discovery process, quest agents change their locations according to the randomly chosen sea lion. However, $\vec{c}$ is larger than one negative value, it forwards the sea lions to identify various prey from a whole search agent. Eq. (13) and Eq. (14) can be represented as follows.

$$\vec{D}_2 = \left| 2\vec{H}.s_{rnd}(\vec{t}) - s(\vec{t}) \right| \tag{13}$$

$$s(t+1) = s_{rnd}(t) - \vec{D}.\vec{c} \tag{14}$$

Here, $s_{rnd}(t)$ refers to the random sea lion that is chosen from the recent population.

The procedure of the adopted ADSLnO model is as follows: Conventionally, the distance update of a sea lion is performed by 3 different distance updates. As per the proposed ADSLnO algorithm, the average distance is calculated for the distance of the tracking phase and the distance of the exploration phase as per Eq. (15), where, D_1 indicates the distance update of the exploration phase, and D_2 denotes the distance update of tracking phase.

$$D = \frac{D_1 + D_2}{2} \tag{15}$$

Algorithm: Proposed ADSLnO method
Initialization
Select D_1 and D_2
Calculate the fitness function as per Eq. (6)
if $(t < \max iter)$
calculate $S\vec{P}_{leader}$ as per Eq. (20)
If($S\vec{P}_{leader}$ <0.25)
If ($c < 1$)
Update the position of the current search agent by Eq. (8)
else
Update the position of the current search agent by Eq. (14)
End if
else
Update the position of the current search agent by Eq. (12)
End if
If the search agent ≠ $S\vec{P}_{leader}$
Go to the first if condition
else
Calculated the fitness function to all search agent
Calculate the average distance as per Eq. (15)
Return s , (i.e.) the best solution
End if
End if
stop

5. DTW for Time Series Classification

From the given input discrete outputs, it is feasible to define the relationship between the two. The process is determined as the classification issue. Euclidean distance evaluation is the key measure to find the similarity among the categories. This is known under the classification rule as well. Let us assume a two-time series Z and O of the same length n. Here $Z = z_1, z_2, ...z_q$ and $O = o_1, o_2, ...o_q$. The Euclidean distance among them 'q' is evaluated as in Eq. (16).

$$d(Z,O) = \sqrt{\sum_{k=1}^{q} (z_k - o_k)^2} \tag{16}$$

When there is an equal length for a two-time series, the distance evaluation could express the similarity very well. Unfortunately, the time-series data falls with different lengths as they are acquired from different natural years. That is why the time series curve of features in the different years often could not attain exact time alignment. Hence, the Euclidean distance might not measure the similarity, which may result in error classification. DTW can determine the proper nonlinear alignment among the time series. While considering the time series Z and O with i and j length, initially construct the $i \times j$ matrix whose $t^k HS, e^k HS$ element is the Euclidean distance among z_t and o_e. It is necessary to identify the path through the matrix, which also reduces the cumulative distance. Then the path determines the optimal alignment.

Let the path be W, where $W = X_1, X_2 ....X_U$ each element W indicates the distance among the point in Z and O as shown in Eq. (17). The rules followed in DTW are given in Eq. (18).

$$X_U = \sqrt{(z_t - o_e)^2} \tag{17}$$

$$DTW(Z,O) = \frac{1}{G} * \min\left(\sum_{U=1}^{G} X_U\right) = \frac{1}{G} * \gamma_U = \frac{1}{G} * \gamma(t,e) \quad (18)$$

In Eq. (3), g is utilized to compensate the regular path of varied length, which should satisfy the condition $\max(i,j) \le G \le i + j + 1$, γ_U indicates the minimum cumulative distance. This is summarized as the recursive function given in Eq. (19). As per this equation, DTW classifies the long time series data.

$$\gamma(t,e) = \sqrt{(z_t - o_e)^2} + \min\left(\gamma(t-1,e-1), \gamma(t-1,e), \gamma(t,e-1)\right) \quad (19)$$

6. Results and Discussions

6.1 Simulation Procedure

The adopted land cover change detection with OCED-ADSLnO model was implemented in MATLAB and their simulation results were observed. The dataset was collected from "https://www.eorc.jaxa.jp/ALOS/en/palsar_fnf/fnf_index.htm". The collected images are illustrated in Fig. 4. The performance of the adopted OCED-ADSLnO model was computed over the traditional schemes like OCED-WOA [41], OCED-SLnO [25], and OCED-GWO [40], respectively. Further, the performance was calculated by varying the learning rate from 1 to 4 in terms of certain measures like F1-score, accuracy, FPR, sensitivity, MCC, specificity, FDR, precision, NPV, and FNR, respectively. Moreover, the change point detection is represented in Fig. 5.

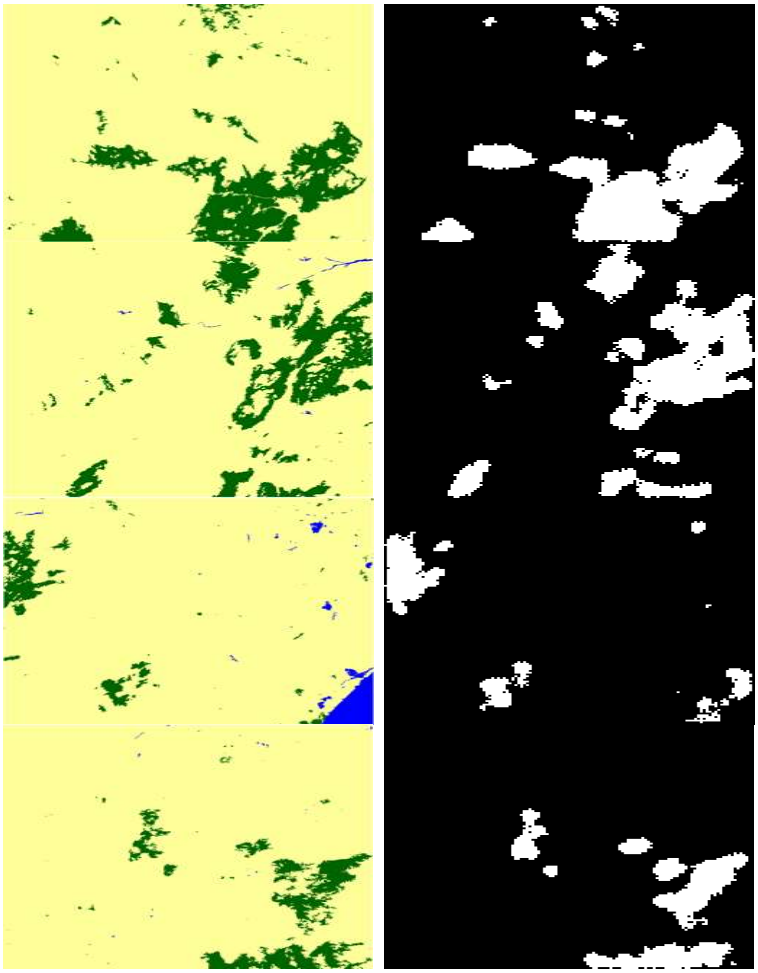

(a) (b)

Fig.4.*Collected images: (a) samaple images (b) segmented iamges*

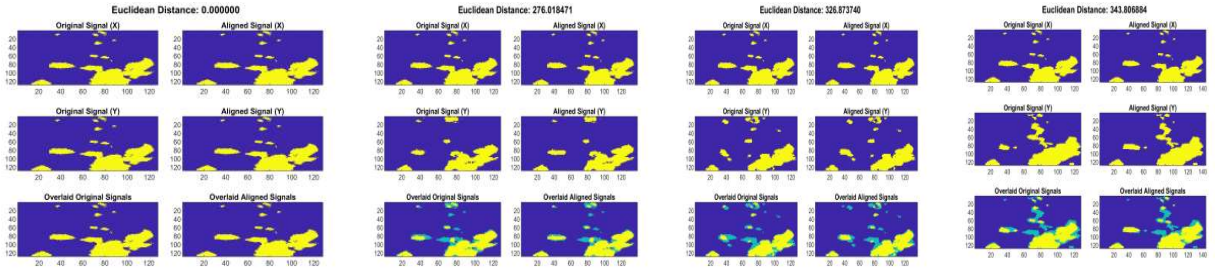

(a) (b) (c) (d)

Fig.5.*Change point detection: (a) 2007-2007 (b) 2007-2009 (c) 2007-2015 (d) 2007-2017*

6.2 Performance Analysis by varying Learning Rate

Fig. 6, 7, and 8 illustrate the performance analysis of the adopted OCED-ADSLnO model over the conventional schemes like OCED-WOA, OCED-SLnO, and OCED-GWO, respectively with respect to different metrics. The results with respect to positive measures are shown in Fig. 6. The results show the performance of accurate change detection when compared to other models almost for all learning rate. Particularly, the accuracy of the proposed OCED-ADSLnOmethod is 1.34%, 1.67%, and 0.33% better than the existing models like OCED-WOA, OCED-SLnO, and OCED-GWO, respectively, for learning rate 2 in Fig 6(c). Likewise, the proposed OCED-ADSLnOmethod in Fig. 6(d) obtains better sensitivity (~0.895); however, the existing schemes like OCED-WOA, OCED-SLnO, and OCED-GWO, respectively hold the lowest values for learning rate 4. The proposed OCED-ADSLnOmodel attains better specificity values when compared to the existing models like OCED-WOA, OCED-SLnO, and OCED-GWO, respectively for learning rate 2 as in Fig. 6(a). In addition, the adopted OCED-ADSLnO algorithm holds maximum precision values for learning rate 1 than other traditional models like OCED-WOA, OCED-SLnO, and OCED-GWO, correspondingly in Fig. 6(b). Thus the improvement of the proposed OCED-ADSLnOmethod is observed clearly for detecting the land cover changes.

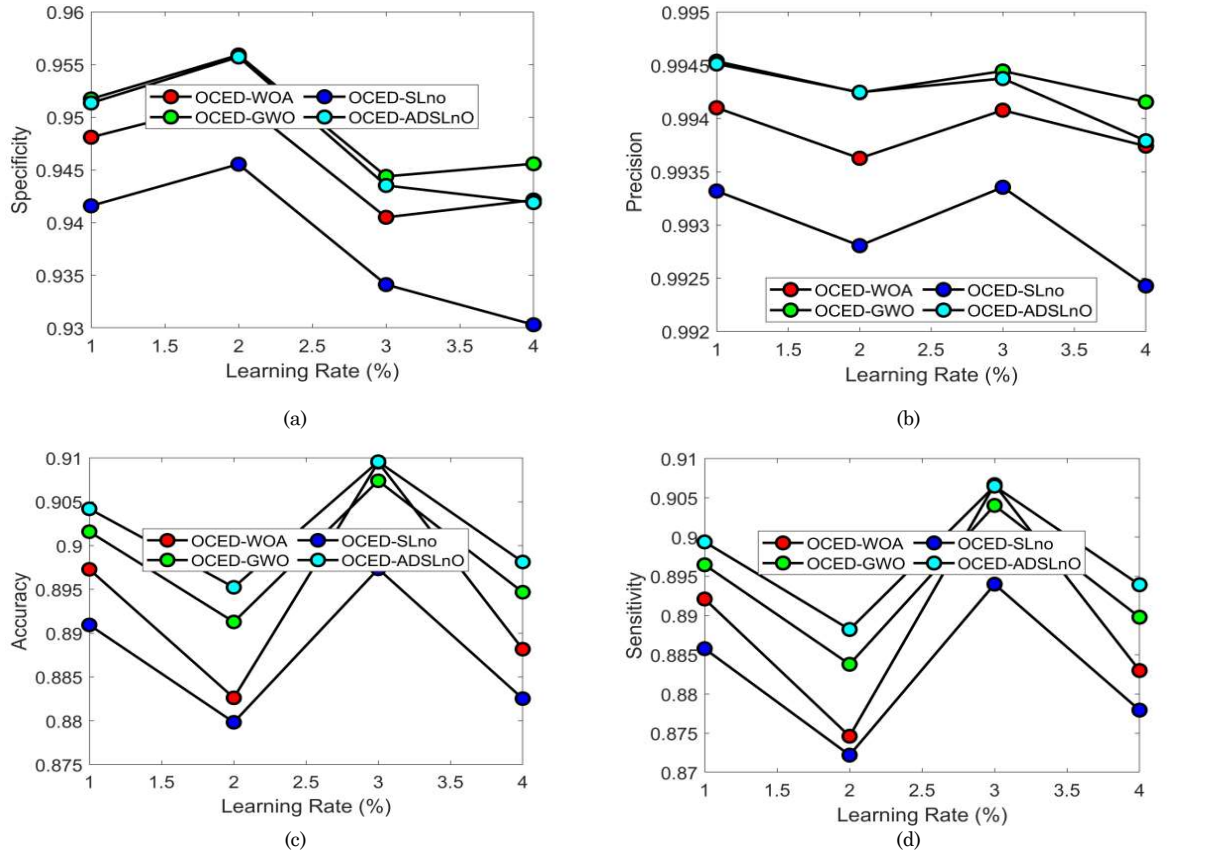

Fig.6.*Performance analysis of the adopted OCED-ADSLnO method over other conventional schemes for (a) specificity (b) precision (c) accuracy (d) sensitivity*

The negative measures analysis of the adopted OCED-ADSLnO model and existing schemes is revealed in Fig. 7. The negative measures such as FDR, FNR, and FPR must be lower for obtaining superior performance. Further, the FPR of the proposed OCED-ADSLnOmethod achieves superior outcomes than other existing models like OCED-WOA, OCED-SLnO, and OCED-GWO, respectively for learning rate 2 as in Fig. 7(a). The proposed OCED-ADSLnOmethod holds a minimum FNR value of (~0.1) for learning rate 1; whereas, the traditional modelsattain: OCED-WOA (~0.108), OCED-SLnO (~0.104), and OCED-GWO (~0.115), respectively in Fig. 7(b). Like wise, the proposed model attains minimum FDR for learning rate 2, which is 7.27%, and 20% better than the other conventional models such as OCED-WOA, and OCED-SLnO, respectively in Fig. 7(c). Thus, the betterment of the adopted OCED-ADSLnO model is proved with minimal error rate.

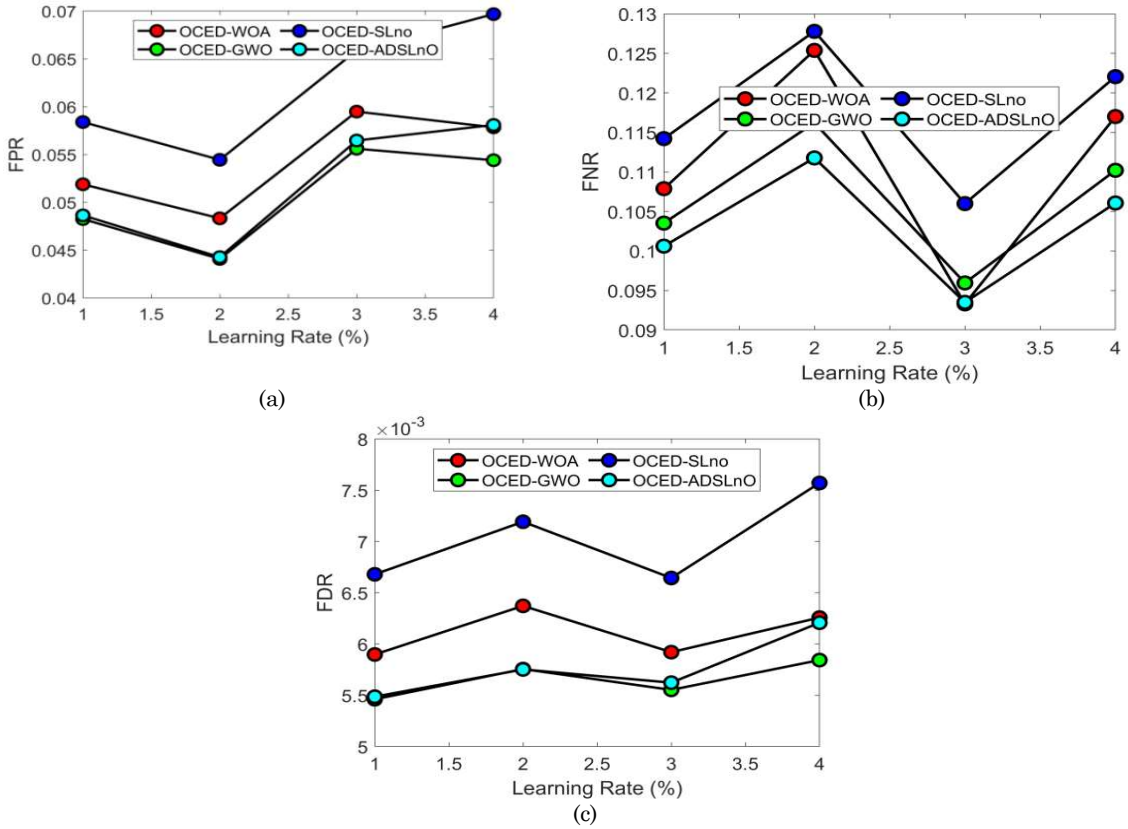

Fig.7.*Performance analysis of the adopted OCED-ADSLnO method over other conventional schemes for (a) FPR (b) FNR (c) FDR*

Fig. 8 illustrates the performance analysis on other measures of the proposed and existing models. In Fig 8(b), the F1-score of the adopted OCED-ADSLnO method for learning rate 3 holds maximum values than other existing models such as OCED-WOA, OCED-SLnO, and OCED-GWO, respectively. The proposed OCED-ADSLnO method holds better NPV value (~0.955) for learning rate 2; whereas the compared existing models like OCED OCED-WOA, OCED-SLnO, and OCED-GWO, respectively attain lower values as in Fig. 8(a). Further, the adopted OCED-ADSLnO model holds higher MCC values than the conventional models like as OCED-WOA, OCED-SLnO, and OCED-GWO, correspondingly at learning rate 4 in Fig. 8(c). Finally, it is observed that the performance of the proposed work is really good for detecting the changes of land from the given time series data, whereas the conventional model shows its poor performance.

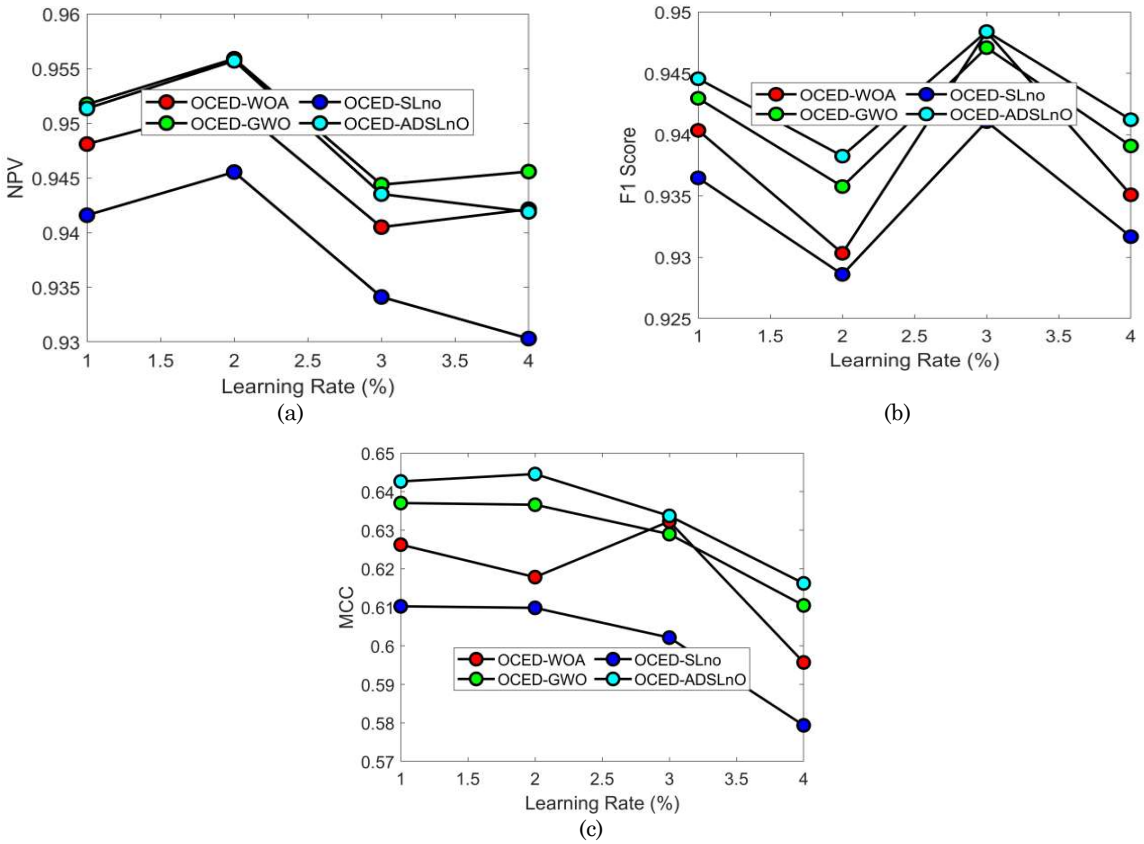

Fig.8.*Performance analysis of the adopted OCED-ADSLnO method over other conventional schemes for (a) NPV (b) F1-score (c) MCC*

6.3 Overall Performance Analysis

The overall performance of the adopted OCED-ADSLnO over CNN [38], and DBN [39] for various measures is summarized in Table II. From the table, the proposed OCED-ADSLnO model has proved its better land cover change detection with respect to various measures than other existing models like CNN, and DBN, respectively. Specifically, the proposed OCED-ADSLnO model attains high accuracy of 89% than other traditional models like CNN, and DBN, respectively, which is given in Table II. Similarly, the FNR, FPR, and FDR of the proposed OCED-ADSLnO method attain less value than other existing schemes, with 0.005 FDR value. Altogether, it is proved that the performance of the proposed model is good than the conventional classifiers like CNN and DBN, respectively in detecting the changes of land image.

Table 2. *Overall performance analysis of adopted and existing schemes*

Metrics	CNN [38]	DBN [39]	OCED-ADSLnO
Accuracy	0.8152	0.88496	0.89524
Sensitivity	0.80205	0.93844	0.88823
Specificity	0.92854	0.42404	0.95572
Precision	0.98977	0.93351	0.99425
FPR	0.071464	0.57596	0.044283
F1-score	0.88608	0.93597	0.93825
MCC	0.50005	0.37006	0.64458
FNR	0.19795	0.061555	0.11177
NPV	0.92854	0.42404	0.95572
FDR	0.010234	0.066488	0.005752

7. Conclusion

In this paper, a new land cover change detection model was implemented with three major three processes: Pre-processing, Detection of forest region, Change detection of the forest. Initially, the input image was subjected to median filtering for outlier removal, reducing the influence of low-quality data

and also filters the noise. Once the image gets pre-processed, it was subjected for the detection of forest in the image by the OCED. The OCED classifier separates the forest region from the image as it resides with the cover of land, water, and forest as well. To make the process more effective, OCED gets enhanced by tuning the weight, and activation function were fine-tuned by the new algorithm termed as ADSLnO algorithm. Subsequently, the detected forest region was subjected to DTW-based time-series classification, which makes the year-wise change detection of the years 2007, 2009, 2015 and 2017. Finally, the performance of the adopted model was analyzed over other existing approaches in terms of certain metrics such as NPV, sensitivity, FDR, accuracy, specificity, FPR, precision, MCC, FNR, and F1-score, respectively. On observing the graph, the accuracy of the adopted OCED-ADSLnO model was 1.34%, 1.67%, and 0.33% better than the existing models like OCED-WOA, OCED-SLnO, and OCED-GWO, respectively, for learning rate 2.The proposed OCED-ADSLnO method holds minimum FNR value of (~0.1) for learning rate 1; whereas, the traditional models holds the value for OCED-WOA (~0.108), OCED-SLnO (~0.104), and OCED-GWO (~0.115), respectively. The proposed OCED-ADSLnO method holds better NPV value (~0.955) for learning rate 2; whereas the compared existing models like OCED OCED-WOA, OCED-SLnO, and OCED-GWO, respectively attains lower values. Thus, the improvement of proposed model was attained effectively.

Compliance with Ethical Standards

Conflicts of interest: Authors declared that they have no conflict of interest.

Human participants: The conducted research follows the ethical standards and the authors ensured that they have not conducted any studies with human participants or animals.

References

[1] Jining Yan, Lizhe Wang, Weijing Song, Yunliang Chen, Ze Deng, "A time-series classification approach based on change detection for rapid land cover mapping", ISPRS Journal of Photogrammetry and Remote Sensing, vol.158, pp. 249-262, December 2019.

[2] Etse Lossou, Nat Owusu-Prempeh, Godwin Agyemang, "Monitoring Land Cover changes in the tropical high forests using multi-temporal remote sensing and spatial analysis techniques", Remote Sensing Applications: Society and Environment, vol.16, November 2019, Article 100264.

[3] Wenqiang Xi, Shihong Du, Yi-Chen Wang, Xiuyuan Zhang, "A spatiotemporal cube model for analyzing satellite image time series: Application to land-cover mapping and change detection", Remote Sensing of Environment, vol. 231, 15 September 2019, Article 111212.

[4] Ziwei Deng, Xiang Zhu, Qingyun He, Lisha Tang, "Land use/land cover classification using time series Landsat 8 images in a heavily urbanized area", Advances in Space Research, vol. 63, no. 71, pp. 2144-2154, April 2019.

[5] S. Chakraborty, A. Banerjee, S. K. S. Gupta, P. R. Christensen and A. Papandreou-Suppappola, "Time-Varying Modeling of Land Cover Change Dynamics Due to Forest Fires," in IEEE Journal of Selected Topics in Applied Earth Observations and Remote Sensing, vol. 11, no. 6, pp. 1769-1776, June 2018, doi: 10.1109/JSTARS.2018.2818060.

[6] W. C. Olding, J. C. Olivier, B. P. Salmon and W. Kleynhans, "A Forecasting Approach to Online Change Detection in Land Cover Time Series," in IEEE Journal of Selected Topics in Applied Earth Observations and Remote Sensing, vol. 12, no. 5, pp. 1451-1460, May 2019, doi: 10.1109/JSTARS.2019.2905594.

[7] Lan H. Nguyen, Deepak R. Joshi, David E. Clay, Geoffrey M. Henebry, "Characterizing land cover/land use from multiple years of Landsat and MODIS time series: A novel approach using land surface phenology modeling and random forest classifier", Remote Sensing of Environment, vol. 238, 1 March 2020, Article 111017.

[8] A. M. Márquez, E. Guevara and D. Rey, "Hybrid Model for Forecasting of Changes in Land Use and Land Cover Using Satellite Techniques," in IEEE Journal of Selected Topics in Applied Earth Observations and Remote Sensing, vol. 12, no. 1, pp. 252-273, Jan. 2019, doi: 10.1109/JSTARS.2018.2885612.

[9] M. H. Elagouz, S. M. Abou-Shleel, A. A. Belal, M. A. O. El-Mohandes, "Detection of land use/cover change in Egyptian Nile Delta using remote sensing", The Egyptian Journal of Remote Sensing and Space Science, vol. 23, no. 1, pp. 57-62, April 2020.

[10] Prabuddh Kumar Mishra, Aman Rai, Suresh Chand Rai, "Land use and land cover change detection using geospatial techniques in the Sikkim Himalaya, India", The Egyptian Journal of Remote Sensing and Space Science In press, corrected proof, Available online 7 March 2019

[11] Jin Xing, Renee Sieber, Terrence Caelli, "A scale-invariant change detection method for land use/cover change research", ISPRS Journal of Photogrammetry and Remote Sensing, vol. 141, pp. 252-264, July 2018.

[12] Huaqiao Xing, Jun Chen, Hao Wu, Jun Zhang, Boyu Liu, "A service relation model for web-based land cover change detection", ISPRS Journal of Photogrammetry and Remote Sensing, vol. 132, pp. 20-32, October 2017. Pp.

[13] Suming Jin, Limin Yang, Zhe Zhu, Collin Homer, "A land cover change detection and classification protocol for updating Alaska NLCD 2001 to 2011", Remote Sensing of Environment, vol. 195, pp. 44-55, 15 June 2017.

[14] Miao Lu, Jun Chen, Huajun Tang, Yuhan Rao, Wenbin Wu, "Land cover change detection by integrating object-based data blending model of Landsat and MODIS", Remote Sensing of Environment, vol. 184, pp. 374-386, October 2016.
[15] Jose L. Gil-Yepes, Luis A. Ruiz, Jorge A. Recio, Ángel Balaguer-Beser, Txomin Hermosilla, "Description and validation of a new set of object-based temporal geostatistical features for land-use/land-cover change detection", ISPRS Journal of Photogrammetry and Remote Sensing, vol. 121, pp. 77-91, November 2016.
[16] [16] Valerio Amici, Matteo Marcantonio, Nicola La Porta, Duccio Rocchini, "A multi-temporal approach in MaxEnt modelling: A new frontier for land use/land cover change detection", Ecological Informatics, vol. 40July 2017 pp. 40-49
[17] Jessica D. DeWitt, Peter G. Chirico, Sarah E. Bergstresser, Timothy A. Warner, " Multi-scale 46-year remote sensing change detection of diamond mining and land cover in a conflict and post-conflict setting", Remote Sensing Applications: Society and Environment, vol. 8, pp. 126-139, November 2017
[18] [18] Md. Inzamul Haque, Rony Basak, "Land cover change detection using GIS and remote sensing techniques: A spatio-temporal study on Tanguar Haor, Sunamganj, Bangladesh", The Egyptian Journal of Remote Sensing and Space Science, vol. 20, no. 2, pp. 251-263, December 2017.
[19] Diego Renza, Estibaliz Martinez, Iñigo Molina, Dora M. Ballesteros L, "Unsupervised change detection in a particular vegetation land cover type using spectral angle mapper", Advances in Space Research, vol. 59, no. 8, pp. 2019-2031, 15 April 2017.
[20] Zhixin Qi, Anthony Gar-On Yeh, Xia Li, Xiaohu Zhang, "A three-component method for timely detection of land cover changes using polarimetric SAR images", ISPRS Journal of Photogrammetry and Remote Sensing, vol. 107, pp. 3-21, September 2015.
[21] Zhe Zhu, Curtis E. Woodcock, "Continuous change detection and classification of land cover using all available Landsat data", Remote Sensing of Environment, vol. 144, pp. 152-171, 25 March 2014.
[22] Swades Pal, Sk. Ziaul, "Detection of land use and land cover change and land surface temperature in English Bazar urban centre", The Egyptian Journal of Remote Sensing and Space Science, vol. 20, no. 1, pp. 125-145, June 2017.
[23] Jesus Aguirre-Gutiérrez, Arie C. Seijmonsbergen, Joost F. Duivenvoorden, "Optimizing land cover classification accuracy for change detection, a combined pixel-based and object-based approach in a mountainous area in Mexico", Applied Geography vol. 34, pp. 29-37, May 2012.
[24] Jun Chen, Miao Lu, Xuehong Chen, Jin Chen, Lijun Chen, "A spectral gradient difference based approach for land cover change detection", ISPRS Journal of Photogrammetry and Remote Sensing, vol. 85, pp. 1-12, November 2013.
[25] Masadeh, Raja & Mahafzah, Basel & Sharieh, Ahmad. "Sea Lion Optimization Algorithm", International Journal of Advanced Computer Science and Applications, vol. 10, pp. 388-395, 2019.
[26] B. R. Rajakumar, "Impact of Static and Adaptive Mutation Techniques on Genetic Algorithm", International Journal of Hybrid Intelligent Systems, vol. 10, no. 1, pp. 11-22, 2013, DOI: 10.3233/HIS-120161.
[27] B. R. Rajakumar, "Static and Adaptive Mutation Techniques for Genetic algorithm: A Systematic Comparative Analysis", International Journal of Computational Science and Engineering, vol. 8, no. 2, pp. 180-193, 2013, DOI: 10.1504/IJCSE.2013.053087.
[28] S. M. Swamy, B. R. Rajakumar and I. R. Valarmathi, "Design of Hybrid Wind and Photovoltaic Power System using Opposition-based Genetic Algorithm with Cauchy Mutation", IET Chennai Fourth International Conference on Sustainable Energy and Intelligent Systems (SEISCON 2013), Chennai, India, Dec. 2013, DOI: 10.1049/ic.2013.0361.
[29] Aloysius George and B. R. Rajakumar, "APOGA: An Adaptive Population Pool Size based Genetic Algorithm", AASRI Procedia - 2013 AASRI Conference on Intelligent Systems and Control (ISC 2013), vol. 4, pp. 288-296, 2013, DOI: https://doi.org/10.1016/j.aasri.2013.10.043.
[30] B. R. Rajakumar and Aloysius George, "A New Adaptive Mutation Technique for Genetic Algorithm", In proceedings of IEEE International Conference on Computational Intelligence and Computing Research (ICCIC), pp. 1-7, Dec 18-20, Coimbatore, India, 2012, DOI: 10.1109/ICCIC.2012.6510293
[31] Srinivasa Rao T C,Tulasi Ram S S,Subrahmanyam J B V, "Enhanced Deep Convolutional Neural Network for Fault Signal Recognition in the Power Distribution System", Journal of Computational Mechanics, Power System and Control, Vol.2,No.3, pp.39-46,2019.
[32] Vinolin V and S Vinusha, "Enhancement in Biodiesel Blend with the Aid of Neural Network and SAPSO", Journal of Computational Mechanics, Power System and Control, Vol.1,No.1, pp.11-17,2018.
[33] Arul.V.H,V.G.Sivakumar,Ramalatha Marimuthu and Basabi Chakraborty, "An Approach for Speech Enhancement Using Deep Convolutional Neural Network", Multimedia Research, Vol.2,No.1, pp.37-44,2019.
[34] Amit Sarkar, "Optimization Assisted Convolutional Neural Network for Facial Emotion Recognition", Multimedia Research, Vol 3, No 2, 2020.
[35] Thomas Thangam, "Adaptive Filter using Improved Pigeon Inspired Optimization algorithm for Satellite Image Denoising", Multimedia Research, Vol 3, No 3, 2020.
[36] Suresh Babu Chandanapalli,Sreenivasa Reddy E,Rajya Lakshmi D, "Convolutional Neural Network for Water Quality Prediction in WSN", Journal of Networking and Communication Systems, Vol.2,No.3, pp.40-47,2019.
[37] Quazi M. H and Dr. S. G. Kahalekar, "Adaptive filtering in EEG Signal for Artifacts Removal using Learning Algorithm", Journal of Networking and Communication Systems, Vol.2,No.2, pp.1-9,2019.
[38] Y. LeCun, K. Kavukvuoglu, and C. Farabet, "Convolutional networks and applications in vision", In Circuits and Systems, International Symposium on, pp.253–256, 2010.

[39] H.Z. Wang, G.B. Wang, G.Q. Li, J.C. Peng, and Y.T. Liu, " Deep belief network based deterministic and probabilistic wind speed forecasting approach", Applied Energy, vol. 182, pp. 80–93, 2016.
[40] Seyedali Mirjalili, Seyed Mohammad Mirjalili, Andrew Lewis, "Grey Wolf Optimizer" Advances in Engineering Software, Volume 69, March 2014, pp. 46-61.
[41] Seyedali Mirjalili, Andrew Lewis, "The Whale Optimization Algorithm" Advances in Engineering Software, vol. 95, pp. 51-67, May 2016.
[42] Khan, R., Li, H., Basir, M., Chen, Y.L., Sajjad, M.M., Haq, I.U., Ullah, B., Arif, M. and Hassan, W., "Monitoring land use land cover changes and its impacts on land surface temperature over Mardan and Charsadda Districts, Khyber Pakhtunkhwa (KP), Pakistan", Environmental Monitoring and Assessment, Vol. 194(6), pp.409, 2022.
[43] Chai, B. and Li, P., "An ensemble method for monitoring land cover changes in urban areas using dense Landsat time series data", ISPRS Journal of Photogrammetry and Remote Sensing, Vol. 195, pp.29-42, 2023.
[44] Tang, Y., Chen, F., Yang, W., Ding, Y., Wan, H., Sun, Z. and Jing, L., "Elaborate Monitoring of Land-Cover Changes in Cultural Landscapes at Heritage Sites Using Very High-Resolution Remote-Sensing Images", Sustainability, Vol. 14(3), pp.1319, 2022.
[45] Xing, H., Wang, H., Zhang, J. and Hou, D., "Monitoring Land Cover Change by Leveraging a Dynamic Service-Oriented Computing Model", Remote Sensing, Vol. 15(3), pp.736, 2023.
[46] Amini, S., Saber, M., Rabiei-Dastjerdi, H. and Homayouni, S., "Urban land use and land cover change analysis using random forest classification of Landsat time series", Remote Sensing, Vol. 14(11), pp.2654, 2022.
[47] Hossain, M.S., Khan, M.A.H., Oluwajuwon, T.V., Biswas, J., Rubaiot Abdullah, S.M., Tanvir, M.S.S.I., Munira, S. and Chowdhury, M.N.A., "Spatiotemporal change detection of land use land cover (LULC) in Fashiakhali wildlife sanctuary (FKWS) impact area, Bangladesh, employing multispectral images and GIS", Modeling Earth Systems and Environment, pp.1-23, 2023.
[48] Shimizu, K., Murakami, W., Furuichi, T. and Estoque, R.C., "Mapping Land Use/Land Cover Changes and Forest Disturbances in Vietnam Using a Landsat Temporal Segmentation Algorithm", Remote Sensing, Vol. 15(3), pp.851, 2023.
[49] Espinoza-Guzmán, M.A., Borrego, D.A. and Sahagún-Sánchez, F.J., "Evaluation of recent land-use and land-cover change in a mountain region. Trees", Forests and People, pp.100370, 2023.